Unaccounted CO_2 leaks downstream of a large tropical hydroelectric reservoir

Elisa Calamita[a,b,1], Annunziato Siviglia[c], Gretchen M. Gettel[d], Mário J. Franca[d,e], R. Scott Winton[a,b], Cristian R. Teodoru[a], Martin Schmid[b], and Bernhard Wehrli[a,b]

[a]Institute of Biogeochemistry and Pollutant Dynamics, ETH Zurich, 8092 Zurich, Switzerland; [b]Department of Surface Waters, Eawag, Swiss Federal Institute of Aquatic Science and Technology, 6047 Kastanienbaum, Switzerland; [c]Department of Civil, Environmental and Mechanical Engineering, University of Trento, 38123 Trento, Italy; [d]IHE Delft Institute for Water Education, 2611 AX Delft, The Netherlands; and [e]Department of Hydraulic Engineering, Delft University of Technology, 2628 CD Delft, The Netherlands

Edited by Andrea Rinaldo, École Polytechnique Fédérale de Lausanne, Lausanne, Switzerland, and approved April 24, 2021 (received for review December 17, 2020)

Recent studies show that tropical hydroelectric reservoirs may be responsible for substantial greenhouse gas emissions to the atmosphere, yet emissions from the surface of released water downstream of the dam are poorly characterized if not neglected entirely from most assessments. We found that carbon dioxide (CO_2) emission downstream of Kariba Dam (southern Africa) varied widely over different timescales and that accounting for downstream emissions and their fluctuations is critically important to the reservoir carbon budget. Seasonal variation was driven by reservoir stratification and the accumulation of CO_2 in hypolimnetic waters, while subdaily variation was driven by hydropeaking events caused by dam operation in response to daily electricity demand. This "carbopeaking" resulted in hourly variations of CO_2 emission up to 200% during stratification. Failing to account for seasonal or subdaily variations in downstream carbon emissions could lead to errors of up to 90% when estimating the reservoir's annual emissions. These results demonstrate the critical need to include both limnological seasonality and dam operation at subdaily time steps in the assessment of carbon budgeting of reservoirs and carbon cycling along the aquatic continuum.

carbon emissions | hydropower dams | river damming | reservoir carbon budget

Inland waters play an important role in the sequestration, transport, and mineralization of carbon (1). Despite recent advances in our understanding of carbon cycling along the aquatic continuum (2–6), major uncertainties remain regarding the impact of human modifications to river hydrology, especially those stemming from large dams (7). Model carbon budgets have been constructed for many artificial reservoirs throughout the world (8); however, a lack of standardized methodologies and criteria for delimiting and attributing dam-driven carbon fluxes has generated biased and unclear metrics for carbon accounting (9). Given an ongoing dam construction boom for hydropower (10, 11), it is therefore an urgent priority to critically reassess carbon cycling within dammed rivers to better understand their role in the inland water carbon balance.

Assessments of hydroelectric reservoir carbon dynamics routinely ignore the importance of "carbon leaks," which arise when carbon released downstream of the dam exceeds the amounts received from inflows (12–16). This "leaked carbon" can be very large relative to other dam-associated carbon emissions, accounting for nearly 90% of the total emissions in one well-documented case in Malaysia (15) and for a substantial contribution (~10–80%) in others (13, 14, 17). These few studies indicate that failure to measure carbon leaks may lead to fundamental misunderstanding of the role of dams and of hydropower development in the carbon biogeochemistry of rivers. There are two main factors that determine the CO_2 emissions downstream of dams: the concentration of dissolved CO_2 in discharged waters and turbulence (18). CO_2 concentration of discharged water is governed by the depth of the outflow in relation to reservoir stratification, which is seasonally dependent and typical in reservoirs with long-enough residence times (19). Turbulence determines the degree to which the water interacts with the atmosphere and therefore the speed at which gas equilibration is reached, i.e., it determines in part the gas-transfer velocity (18). Turbulence downstream links to dam discharge, which can vary substantially throughout the day depending on energy demand—a phenomenon known as "hydropeaking" (20). Given these different sources of variation, an ideal framework for estimating CO_2 leakage would address both subdaily (hourly) and seasonal-scale variations in discharge and CO_2 concentration.

Here, we use a year-long dataset composed of high-frequency measurements of water temperature, pH, and conductivity in the Zambezi River to estimate CO_2 emissions downstream of Kariba Dam (Zambia) and compare them with a reference site upstream of Victoria Falls (upstream of Kariba Reservoir) to assess the relative importance of reservoir stratification and dam operations on downstream CO_2 emissions. We derived a rating curve to estimate hourly water velocity and depth from which we then calculated the gas transfer velocity [k_{600}, k_{CO2} (21)]

Significance

Hydroelectric reservoirs emit substantial amounts of CO_2, especially in the tropics. Since many such systems exist and many more will be built within decades, it is important to assess their role in the carbon cycle. A major source of emission that is rarely monitored and never at different timescales is the carbon released downstream of dams. We measured the seasonal and subdaily variability of CO_2 emission downstream of one of the world's largest artificial reservoirs and find that its contribution is relevant for unbiased quantification of reservoir carbon budgets. These findings highlight the importance of subdaily variability in hydropower operation for downstream emission rates and call for appropriate analysis schemes to reassess the greenhouse gas footprint of this energy source.

Author contributions: E.C., A.S., and B.W. designed research; E.C., A.S., G.M.G., M.J.F., R.S.W., C.R.T., and M.S. performed research; B.W. contributed analytic tools; E.C. analyzed data; and E.C., A.S., G.M.G., M.J.F., R.S.W., C.R.T., M.S., and B.W. wrote the paper.

The authors declare no competing interest.

This article is a PNAS Direct Submission.

This open access article is distributed under Creative Commons Attribution-NonCommercial-NoDerivatives License 4.0 (CC BY-NC-ND).

[1]To whom correspondence may be addressed. Email: Elisa.calamita@usys.ethz.ch.

This article contains supporting information online at https://www.pnas.org/lookup/suppl/doi:10.1073/pnas.2026004118/-/DCSupplemental.

Published June 14, 2021.

Downloaded by guest on June 14, 2021

and subsequently the rate of CO_2 emission to the atmosphere (see *Materials and Methods* and *SI Appendix*). The combination of high-frequency measurements and long-term monitoring allowed us to assess the relative importance of reservoir stratification and dam operations on downstream CO_2 emissions and the magnitude of these emissions compared to other components of a conventional reservoir carbon budget.

Results and Discussion

CO_2 Hotspots Downstream of Large Dams. Dams interrupt the river continuum, and our analysis shows that they can create major discontinuities in CO_2 degassing as well. To evaluate this, we compared the specific emission rate just 3 km downstream of Kariba Dam with the whole Zambezi River, based on earlier field measurements (22). We found that this flux accounts for approximately one-fourth of the specific emission rate of the entire Zambezi River [1,040 mg $C{\cdot}m^2{\cdot}d^{-1}$ downstream of the dam compared to 4,290 mg $C{\cdot}m^2{\cdot}d^{-1}$ for the whole river (22)]. The quantification of this flux allows for calculating the CO_2 leaks.

There are multiple approaches for estimating the total magnitude of carbon emissions downstream of dams. We assess two options for the case of Kariba. The first approach considers degassing rates which, multiplied by the surface area of a predefined downstream river reach, yields the total annual emitted mass (15). A second approach subtracts the total carbon leakage measured at the outflow from the carbon flux into the reservoir. This assumes that essentially all of the dissolved inorganic carbon in excess of that which arrives from river inflows can be attributed to the reservoir and will be emitted to the atmosphere on a short timescale (23, 24). Both approaches lead us to conclude that the carbon leakage from Kariba Dam is important to the overall carbon budget of the Kariba Reservoir (Fig. 1).

The annual CO_2 emission from the Zambezi River downstream of Kariba Dam, calculated by integrating the hourly time series of the CO_2 atmospheric emission (the first approach), equals 377 g $C{\cdot}m^2{\cdot}y^{-1}$ (ranging between 331 and 382 g $C{\cdot}m^2{\cdot}y^{-1}$ depending on estimation methods; see *Materials and Methods*). This emission rate, applied to the Zambezi River between Kariba Dam and the confluence with the Kafue River (the first important discontinuity, located ~75 km downstream; see *SI Appendix*, Fig. S1) would correspond to about 18 Gg $C{\cdot}y^{-1}$ or 7 to 32% of the total net CO_2 uptake (−56 to −278 Gg $C{\cdot}y^{-1}$; F_{CO2} surface of Fig. 1*A*) of Lake Kariba (22–25). Using the second approach, which considers the difference between partial pressure of CO_2 (pCO_2) in the inflows (estimated using CO_2 saturation concentration and water temperature at Victoria Falls; 10 Gg $C{\cdot}y^{-1}$) and the outflows, the estimated carbon leak doubles to 35 Gg $C{\cdot}y^{-1}$ or 13 to 63% of the total net CO_2 uptake of Lake Kariba (Fig. 1). The variability in the importance of carbon leaks reflects the sensitivity to underlying assumptions and the large uncertainty surrounding the other components of the reservoir carbon budget. The magnitude of even the minimal values makes clear, though, that CO_2 outgassing downstream of Kariba Dam is significant and represents an important component of the carbon budget of the reservoir. Moreover, accounting for the CO_2 outgassing at the turbines, here not quantified (due to the lack of the sufficiently highly resolved vertical profiles of CO_2 within the reservoir's water column and the hourly amount of water withdrawn from each withdrawal point), would make the total amount of CO_2 emissions occurring downstream of the dam even higher. This finding indicates that if we continue to omit downstream carbon emissions from assessments of reservoir carbon cycling, we may be systematically underestimating the role of reservoirs in the carbon balance of inland waters.

Seasonality of CO_2 Evasion. Any reservoir that has a prolonged season of stratification and that has sufficiently deep outlet points may discharge downstream hypolimnetic water enriched in CO_2. The mixing regime of reservoirs and their interaction with dam outlet points is therefore a key determinant of the magnitude and seasonal dynamics of downstream carbon emissions. We found that river water downstream of Kariba Dam was always oversaturated with CO_2. However, concentrations varied seasonally in response to stratification dynamics [seasonal stratification occurring between October and June and experiencing its maximum in February (26); Fig. 2*A*] from a minimum of 470 ppm, at the end of the reservoir mixing phase, to a maximum of 6,810 ppm at the beginning of the year, after CO_2 has accumulated over several months in the hypolimnion. High CO_2 concentration was also observed during the beginning of the mixing phase (July; Fig. 3*B*), when CO_2-rich hypolimnetic water is mixed into the epilimnion, resulting in elevated concentrations at the level of the water intakes to all turbines. This results in a range of CO_2 emissions rates downstream spanning two orders of magnitude, from 24 to 3,730 mg $C{\cdot}m^2{\cdot}d^{-1}$ (mean value of about 1,040 mg $C{\cdot}m^2{\cdot}d^{-1}$; Fig. 2*B*). Moreover, the observed fluctuations in CO_2 concentrations and emissions which we observed show a completely different seasonality compared to those upstream of Lake Kariba and at the Victoria Falls (Fig. 3*B*), where the seasonality of dissolved CO_2 relates to the floodplain dynamics, with maximum loads during peak flow condition (27).

Carbopeaking Linked to Dam Management. In addition to the seasonal variation observed in CO_2 concentration and outgassing, subdaily fluctuations driven by hydropower operation is also a significant source of variability. Previous work demonstrates that hydropeaking events can generate subdaily alterations in river water temperature, a process called "thermopeaking" (28, 29). Our analysis indicates that a similar link exists between hydropeaking fluctuations and variations in carbon emissions downstream of a dam. We propose the term "carbopeaking" to refer to subdaily fluctuations in CO_2 atmospheric emissions associated with dam hydropeaking (Fig. 4 *A* and *B*).

Conceptually, carbopeaking is driven by variations in transport and concentration: An abrupt rise in water discharge potentially combined with a sudden increase in CO_2 concentration in the downstream river results in an ephemeral peak of CO_2 emissions to the atmosphere (Fig. 1 *B* and *C*). To date, the effect of hydropeaking on the water–air CO_2 exchange and more generally on the carbon budgets at the annual scale has never been considered, mainly because the CO_2 atmospheric emission of regulated rivers is often not measured at the subdaily timescale but rather calculated based on a few samples per year. However, we demonstrate that dam operation affects the temporal dynamics of CO_2 emission below dams and can generate large fluctuations of such emission.

Our subdaily measurements from below Kariba Dam provide direct evidence for the occurrence of carbopeaking. Rapid operational shifts at Kariba, related to energy demand, form two peaks in hydropower production each day: in the morning between 6 and 10 AM and in the early evening between 6 and 8 PM. The rate of change in discharge downstream of Kariba Dam reaches values up to ~550 $m^3{\cdot}s^{-1}{\cdot}h^{-1}$—a magnitude that amounts to 30% of the yearly average discharge (1,500 $m^3{\cdot}s^{-1}$). Because this change in discharge in the case of Kariba Dam is associated with multiple turbine intakes located at different depths, the concentration of CO_2 also varies with discharge, reaching a maximum change rate of 2,140 $ppm{\cdot}CO_2{\cdot}h^{-1}$ (see *Materials and Methods*). The combined effect of varying discharge and CO_2 concentration downstream of Kariba Dam generates subdaily fluctuations in CO_2 emissions four times

Downloaded by guest on June 14, 2021

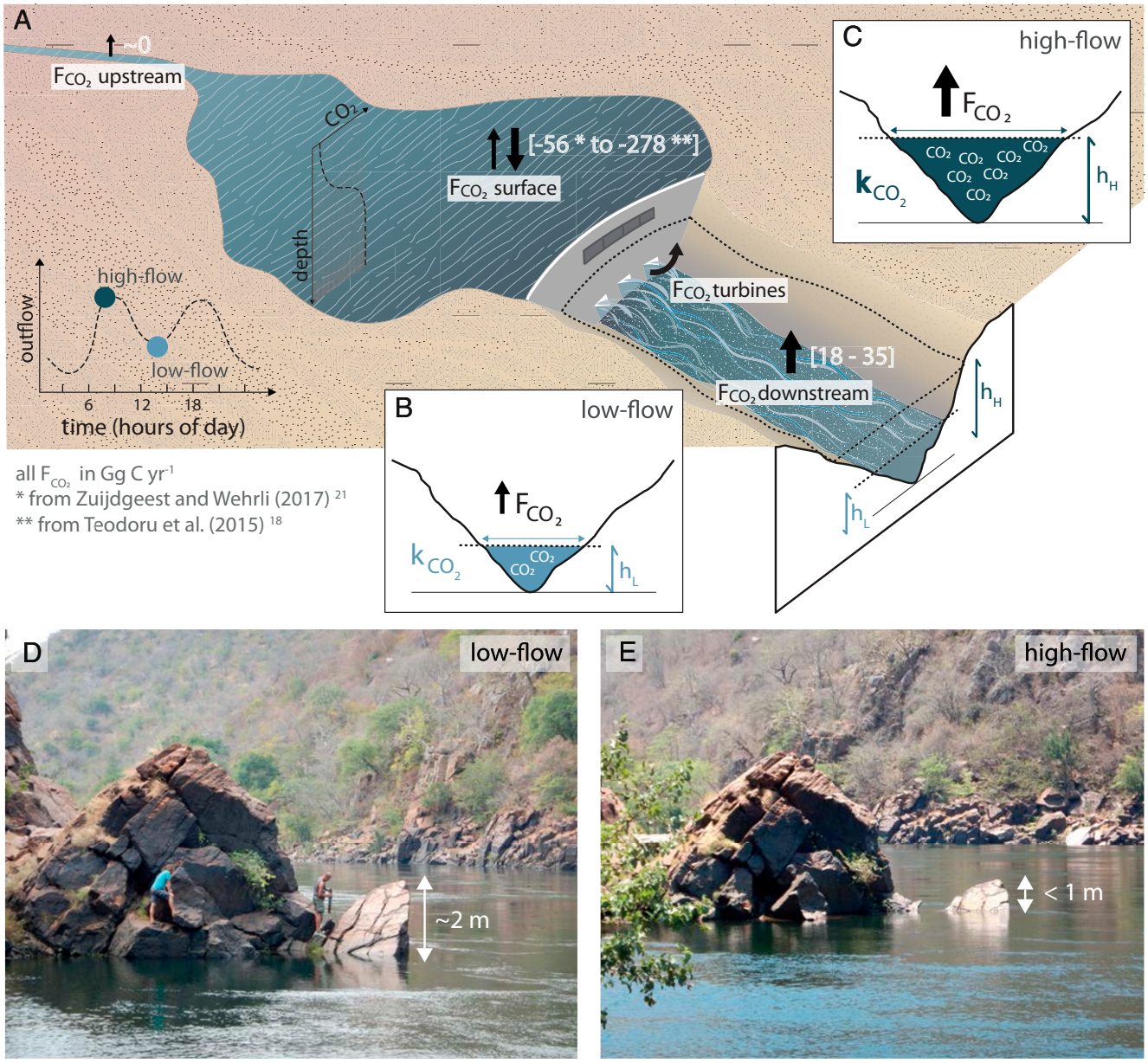

Fig. 1. Pathways of CO_2 emissions to the atmosphere from a river–reservoir system including the downstream emission hotspot and their quantification for the Zambezi River–Kariba system. (*A*) Reservoir-related CO_2 emissions differentiated between emissions across the surface (F_{CO2} surface) of the standing water body and emissions that occur downstream of the dam resulting from degassing at the turbines (F_{CO2} turbines) or through evasion of the remaining excess gas in the downstream river (F_{CO2} downstream). The magnitude of the latter depends on the stratification of the reservoir and hydropower operation (positive fluxes are from the waterbody to the atmosphere). The release of hypolimnetic CO_2-oversaturated water together with hydropeaking (*D* and *E*; photos taken 3 km downstream of Kariba Dam) generates carbopeaking, subdaily fluctuations of the CO_2 flux through the river's surface. (*B*) During low flow, the lower water–air gas exchange velocity and the smaller water–air interface reduce the outgassing. Vice versa, (*C*) during high flow the higher turbulence generating higher water–air gas transfer velocity and the larger water–air interface enhances CO_2 outgassing. Multiintake reservoirs can further enhance carbopeaking by causing fluctuations of CO_2 concentration in the outflow.

greater than those of upstream reference conditions. We found rates of change in hourly CO_2 efflux up to ~870 mg C·m^{-2}·d^{-1}, corresponding to a fluctuation of up to ~200% in 1 h.

Although hydropeaking at Kariba occurred throughout the study year, and consistently contributed to peaks in carbon emissions, carbopeaking was most pronounced during months with reservoir stratification (Fig. 4 *A* and *B*), reaching its apex during the maximum CO_2 accumulation in the reservoir hypolimnion. This indicates that CO_2 concentration rather than turbulence caused by the rate of discharge is the dominant control on carbopeaking (Fig. 4*C*). We also performed a sensitivity analysis considering a constant discharge value and the measured hourly variability in CO_2 concentrations, and we reached the same conclusion that carbopeaking is mainly driven by changes in concentration rather than by changes in discharge. However, we estimate that hydropeaking contributes about 20% to the carbopeaking we observe at Kariba (Fig. 4*C*), and its role is even more important if we consider that when the water discharge increases so does the water level (up to 2 m·h^{-1} at the location of our sensor) and therefore the area of the river and the air–water

Downloaded by guest on June 14, 2021

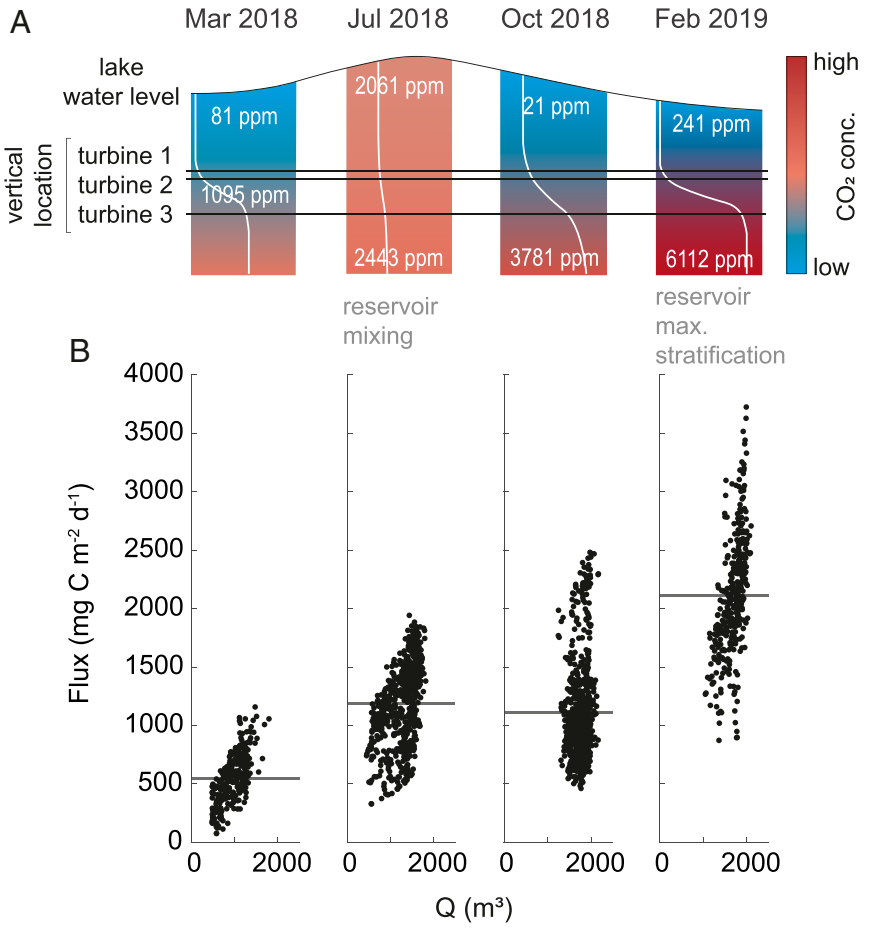

Fig. 2. Reservoir CO_2 concentration in response to stratification dynamics generates seasonal variability of CO_2 atmospheric emission from the Zambezi River downstream of the dam wall. (*A*) Measured epilimnetic and hypolimnetic (or metalimnetic for March 2018) concentration of CO_2 in the water column of Lake Kariba just behind the dam on 18 March 2018, 9 July 2018 (lake mixing), 30 October 2018, and 16 February 2019 (maximum stratification of Lake Kariba) together with the water level in the reservoir and the relative depth of the intake of the three turbines. (*B*) Calculated degassing flux from the Zambezi River 3 km downstream of Kariba Dam (see *Materials and Methods* and *SI Appendix*) as a function of water discharge (Q) during the same four months. Gray lines indicate the monthly mean CO_2 flux.

interface (up to 15% at the location of our sensor), resulting in a proportionately higher total flux escaping the river surface per unit of time (Fig. 1). Thus, carbopeaking potentially occurs downstream of many stratified dams operating with a hydropeaking regime worldwide. Moreover, such a link between power production peaks and CO_2 emissions shows that explicitly considering dam operations may be necessary for accurately calculating the CO_2 storage in reservoirs and a more complete understanding of the role of the aquatic continuum in global carbon cycling.

Timescales Matter for Carbon Budgeting. Scientists have called for increased monitoring of greenhouse gas emissions associated with hydropower reservoirs in the tropics to reassess the greenhouse gas footprint of this energy source (30, 31). We argue that it is critically important to include measurements of downstream carbon emissions at relevant timescales in order to accurately estimate carbon budgets for reservoirs. These timescales should include seasonal changes in CO_2 concentration in the reservoir but also subdaily peaks associated with dam operation. With an automated sensor at Kariba Dam we were able to integrate hourly data and estimate an annual downstream emission of 377 g $C{\cdot}m^2{\cdot}y^{-1}$. These findings highlight the potential errors associated with estimating annual emissions based on a single survey which could potentially overestimate emissions by up to 30% or underestimate emissions by up to 90% (see *SI Appendix*). Thus, monitoring carbon flux from dam tailwaters must be informed by the seasonality of mixing and CO_2 concentrations in the reservoir. In a review of large tropical hydropower reservoirs, 34 out of a total of 36 assessed reservoirs stratify, which shows the potential for this to be a significant error on estimates of CO_2 emissions and carbon budgets for hydropower reservoirs (19). Hence, one or two measurements in a year will likely lead to major errors.

In addition to seasonal variability, our analysis of carbopeaking below Kariba Dam indicates the importance of accounting for subdaily fluctuations in discharge to avoid systematic errors in upscaling. Measurements taken during one of the two daily hydro-/carbopeaks (midmorning, early evening) will be biased toward overestimation, whereas measurements taken during low discharge (predawn) will be biased toward underestimation (Fig. 5). A diligent surveyor could theoretically measure CO_2 flux monthly, weekly, or even daily, for maximum coverage of seasonality, and still yield a difference of up to 30% depending on how the timing of sampling was to align with carbopeaking patterns (Fig. 5). We find that accounting for carbopeaking dynamics is key to avoid biased estimates of carbon emission hotspots below dams.

Hydroelectric reservoirs are often used to flexibly produce electricity when demand is high and supply from other sources is

Downloaded by guest on June 14, 2021

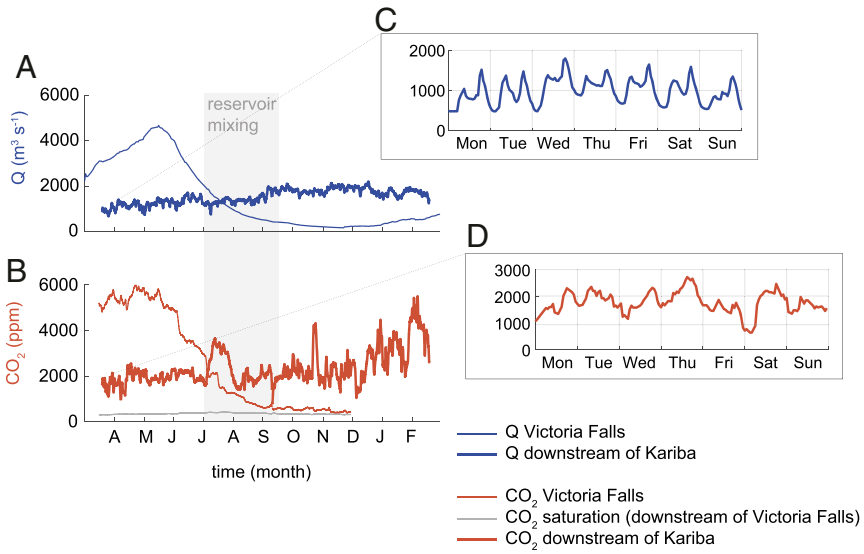

Fig. 3. Altered seasonality and enhanced subdaily fluctuations of water discharge (Q) and CO_2 concentration in the Zambezi River 3 km downstream of Kariba Dam. Yearly signal (*A* and *B*) (smoothed with time window of 24 h) and hourly fluctuations (*C* and *D*) of reconstructed water discharge (*A* and *C*) and calculated CO_2 concentration (*B* and *D*) in the Zambezi River 3 km downstream of Kariba Dam (thick lines) and upstream of the Victoria Falls (thin lines). See *Materials and Methods* and *SI Appendix* for calculation details.

insufficient; thus, their power production can be highly variable within a day, which causes significant subdaily flow fluctuations and increases the likelihood of carbopeaking worldwide. Among tropical rivers, our case study, the Zambezi River, is not the only documented example where hydropeaking occurs; hydropeaking has been documented in the Amazon Basin (32) and substantial subdaily flow variability has been reported downstream of the Malaysian Batang Ai Dam (33). Thus, it is necessary to have well-resolved temporal monitoring, not only of the surface fluxes (34) but also for the downstream emissions, in order to provide reliable reservoir carbon budgets. Even for the cases where the downstream emissions have been included, fluxes have been

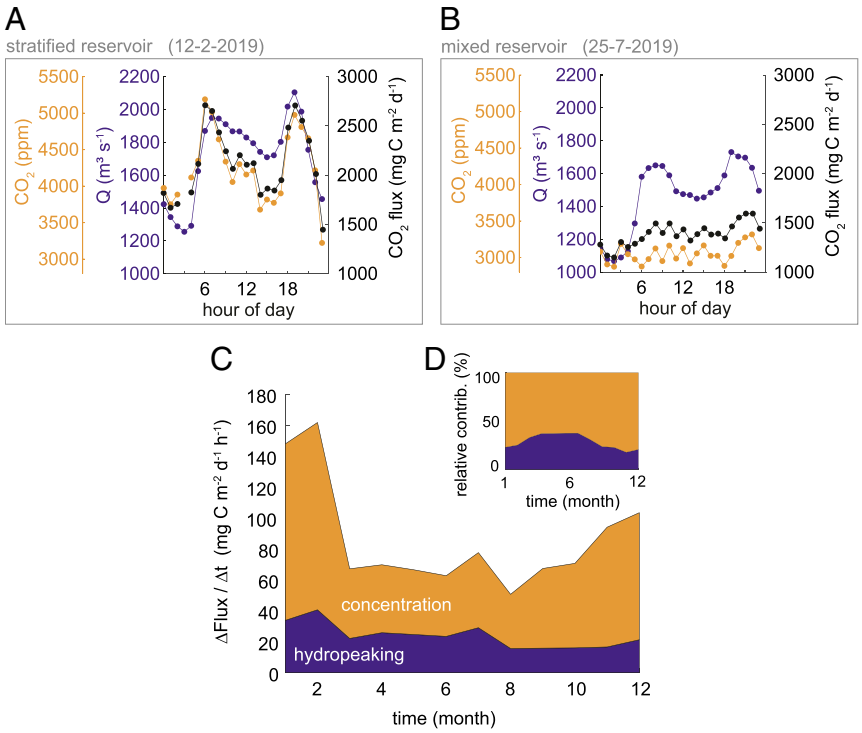

Fig. 4. Carbopeaking is caused by hydropeaking and fluctuations of CO_2 dissolved concentration. (*A* and *B*) Hourly water discharge (Q) and calculated CO_2 concentration and flux during two specific days of the year: during Kariba's reservoir stratified season (12 February 2019) and during its mixed phase (25 July 2019). (*C*) Mean monthly carbopeaking absolute values (hourly variations of CO_2 atmospheric emission) together with the contribution of hydropeaking and concentration to the respective monthly carbopeaking value. (*D*) Monthly relative contributions of hydropeaking and concentration to carbopeaking.

Downloaded by guest on June 14, 2021

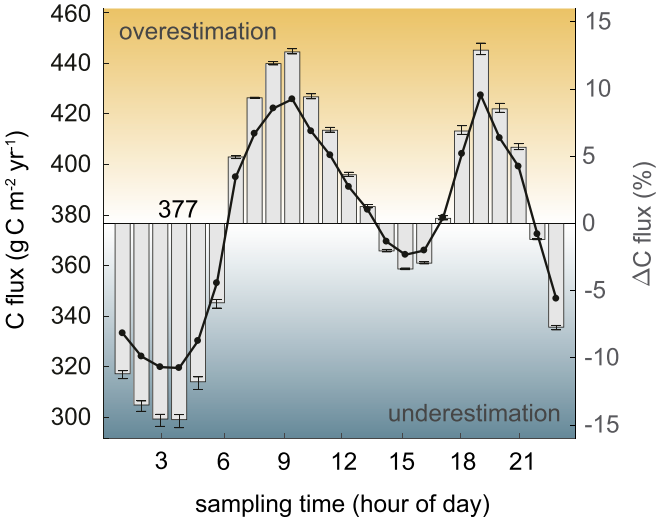

Fig. 5. Error in the calculation of the annual atmospheric CO_2 emission downstream of the Kariba Dam generated by ignoring carbopeaking. Yearly CO_2 emission flux downstream of Kariba Dam calculated using the hourly time series (horizontal line, 377 g $C{\cdot}m^{-2}{\cdot}y^{-1}$) and the same flux calculated just using measurements at a certain time of the day indicated in the abscissa (black line). The bar plot shows the relative difference (in percentage) between the yearly flux estimated by using measurements at a certain hour of the day and the total integral of the hourly CO_2 atmospheric emission. Error bars show the difference between the three different models used to calculate the CO_2 atmospheric emission. See *Materials and Methods* and *SI Appendix*.

based on only a few samples per year, and our work shows that these estimates may be highly biased given the high subdaily fluctuations (15, 33). Having a well-resolved temporal CO_2 estimate of the downstream emissions would also refine the global estimates of carbon emissions from hydroelectric reservoirs which currently often neglect the downstream emissions because their measurements are too limited and/or too poorly constrained to be meaningfully included in global upscaling efforts (8).

Both seasonal and subdaily measurements would be part of an ideal framework for estimating carbon emissions from the river water surface below stratifying artificial reservoirs subjected to high CO_2 concentration in the hypolimnion. The availability of automated sensors capable of high-frequency measurements and long-term deployments make such an ideal framework realizable. The present study focused on CO_2, but methane (CH_4) is an even more potent greenhouse gas (35) which also accumulates in the hypolimnia of lakes and then can be emitted to the atmosphere (8, 36, 37), and its emission from the reservoir surface can vary daily (38). Future research into the carbon cycling of dams and the emission hotspots downstream should therefore also assess methane fluxes in the downstream river system and their seasonal and subdaily variation.

Materials and Methods

Study Site. This study focuses on a 75-km reach of the Middle Zambezi River, from Kariba Dam to the confluence with the Kafue River. This is a low-gradient sand-bed river reach which has single-thread and braided channel patterns. The river's slope (s) ranges from 1×10^{-4} to 3×10^{-4}, and the river's width from 150 to 1,800 m. The flow velocity (v) depends on the discharge released by the dam and ranges between 0.3 and 2.5 $m{\cdot}s^{-1}$. The estimated energy dissipation rate ($eD = g \cdot v \cdot s$, where g is the gravitational acceleration) ranges between 3×10^{-3} and 7×10^{-3} $m^2{\cdot}s^{-3}$. Kariba Dam and its hydropower plant are transboundary structures, with management shared between Zambia and Zimbabwe. The Zambian hydropower station is equipped with six turbines and the Zimbabwean station has eight turbines. Moreover, the dam is equipped with six spilling gates for controlling the water level, but they are not in use because of structural problems of the dam. The turbine water intakes and the spilling gates are located at different depths: The sill elevations of the turbine intakes on the Zimbabwean side are at 447 m above sea level (a.s.l.) for the low-level intakes and 460 m a.s.l. for the high-level intakes; on the Zambian side the intakes are at 460 m a.s.l. and the six spilling gates at 457 to 466 m a.s.l. (39).

Sensor Deployment and Sampling. We monitored water quality by deploying three EXO2 probes (Yellow Springs Instruments) along the Middle Zambezi River at three distinct locations: the first one at Siavonga, 3 km downstream of Kariba Dam wall (latitude = 16.50441 S; longitude = 28.79071 E), the second one upstream of the Victoria Falls to have a reference condition of the Zambezi River (latitude = 17.82075 S; longitude = 25.65795 E), and the third one at Chirundu, about 75 km downstream of Kariba Dam (latitude = 15.98481 S; longitude = 28.88075 E). The EXO2 probes measured and recorded water temperature (T), conductivity (EC), pH, and dissolved oxygen (DO) from mid-March 2018 until the end of February 2019 with an hourly time resolution. The first probe was moored from a rock positioned roughly 2 m above the riverbed, so this probe also recorded the water-level fluctuations, while the other two were installed on floating mode (pontoon and buoy) and so kept a constant depth of ~1 m relative to the surface. Approximately every 3 mo all probes were recalibrated for pH and DO using standard buffer solutions of pH 4 and pH 7 and water-saturated air, respectively. We used all calibration values to correct the data in postprocessing for possible drift in measured parameters.

In situ measurements and water samples were taken at various locations along the Zambezi River Basin to address the longitudinal variability and the influence of tributaries and to cross-validate the EXO2 probe measurements. We sampled 17 locations (including the EXO2 locations) along the Zambezi River and its tributaries and the surface and hypolimnion of Lake Kariba close to the dam wall in March, July, and November 2018 and February 2019. At each location we measured water temperature, DO, conductivity, and pH using YSI ProPlus and YSI ProODO multimeter probes (Yellow Springs Instruments). The pH and DO probes were calibrated before each measurement using standard buffer solutions of pH 4 and pH 7 and water-saturated air, respectively.

Moreover, we collected samples for alkalinity in 50-mL centrifuge tubes and kept them refrigerated until analysis at the Eawag laboratory in Switzerland. We used an 862 Compact Titrosampler (Metrohm) to measure alkalinity.

This full dataset is deposited on the ETH Research Collection data portal under DOI 10.3929/ethz-b-000473097 (40).

CO_2 Concentration Measurements. In all sampling locations, we measured in situ the pCO_2 in the water using an EGM-4 nondispersive, infrared gas analyzer (PP Systems), using the headspace technique. The EGM-4 was calibrated before each trip with certified gas standards of 1,017 ppm CO_2, while 0 ppm CO2 is automatically performed by the instrument running the air through a soda lime absorbed column ("autozero" technology).

For the headspace equilibrium technique, 30 mL of water was collected from 30 to 50 cm below water surface into five 60-mL polypropylene syringes and mixed with 30 mL ambient air of measured CO_2 concentration ($pCO_{2,a}$) then gently shaken for 5 min to allow for equilibration of the two phases. The equilibrated headspace volume (30 mL) was then transferred into a dry syringe and directly injected into the EGM-4 analyzer to measure the partial pressure CO_2 of the headspace in the syringe after equilibration ($pCO_{2,s}$). Water pCO_2 was calculated from the ratio between the air and water volumes using the gas solubility at sampling temperature. The gas solubility (K_0) was calculated as in ref. 41 (assuming zero salinity) for the sampling temperature and for the temperature of the sample after equilibration ($K_{0,s}$, $K_{0,a}$, respectively):

$$\ln K_0 = A_1 + A_2\,(100/T) + A_3 \ln\,(T/100), \qquad [1]$$

where the solubility K_0 is expressed in moles per kilogram per atmosphere; A_1, A_2, and A_3 are constants equal to −60.2409, 93.4517, and 23.3585, respectively; and T is the absolute water temperature in Kelvin. We then calculated the molar volume V_m (liters per mole) from the ideal gas law using the temperature and pressure of the sample. The water sample partial pressure pCO_2 (parts per million) was then calculated as follows:

$$pCO_2 = \left[(pCO_{2,s} - pCO_{2,a})\,\frac{V_h}{V_w P_a V_m} + pCO_{2,s} \cdot K_{0,a}\right]\frac{1}{K_{0,s}}, \qquad [2]$$

Downloaded by guest on June 14, 2021

where V_h and V_w are the volume of the headspace and the volume of water in the syringe, respectively, and P_a is the atmospheric pressure in atmospheres.

Rating Curve and Hydropeaking Characterization. We reconstructed the relative rating curve for the probe located 3 km downstream of the Kariba Dam. For this purpose we used the probe measurements of relative water level fluctuations and the hourly time series of turbinated water provided by the Zambian power station (Zambia Electricity Supply Corporation, ZESCO) and the Zimbabwean power station (Zimbabwean Power Company, ZPC). We performed a fitting using a power model; the data and the resulting relative rating curve are reported in *SI Appendix*, Fig. S2.

Hydropeaking occurred throughout the study year at Kariba, leading to subdaily fluctuations of the Zambezi's CO_2 exchange velocity. Two indicators HP_1 (0.48) and HP_2 (169 $m^3 \cdot s^{-1} \cdot h^{-1}$) (20) characterize hydropeaking at Kariba and confirm its importance: The first is a dimensionless measure of the magnitude of hydropeaking and the second measures the temporal rate of discharge changes.

CO_2 Concentration Calculation. We used the conductivity record to calculate the alkalinity at the hourly time resolution. Conductivity and alkalinity are indeed highly correlated in our case study (see *SI Appendix*, Fig. S3*A*). The correlations between conductivity and alkalinity result from natural geological and climatic controls and are often used to assess anthropogenic impacts on streams or rivers (42, 43). Moreover, such clear correlation between EC and alkalinity in the Zambezi River Basin has been previously reported by Zuijdgeest et al. (27). In a second step we combined the conductivity-based alkalinity data with measured pH, temperature, and salinity and the entire carbonate system was calculated with the CO2SYS* MATLAB script (44). Calculated versus measured CO_2 concentrations show a quite good agreement (R^2 = 0.76; see *SI Appendix*, Fig. S3*B*). However, calculated values exceed measurements, with higher discrepancies generally for high CO_2 values. It is worth noting that, in the absence of other external factors (turbulence, waves, and wind), CO_2 emissions tend to be greater at higher water CO_2 content. In other words, smaller in situ measured CO_2 in comparison to the calculated one is likely due to the unaccounted CO_2 that is lost to the atmosphere at the time of sampling. Such discrepancies have been previously reported for various freshwater systems (45). Calculated CO_2 concentrations for the Zambezi River at Siavonga (3 km downstream of Kariba Dam), Victoria Falls (reference site upstream of Kariba Reservoir), and Chirundu (~75 km downstream of Kariba Dam) are reported in *SI Appendix*, Fig. S1 (see how data gaps due to equipment failure were addressed in *SI Appendix*, Fig. S1 legend).

*https://cdiac.ess-dive.lbl.gov/ftp/co2sys/CO2SYS_calc_MATLAB_v1.1/.

CO_2 Outgassing. The outgassing flux of CO_2 is defined as $F_{CO_2} = k_{CO_2}(C - C_{eq})$, where k_{CO2} is the gas transfer velocity at the air–water interface and $(C - C_{eq})$ is the difference between the actual CO_2 concentration in the water and the dissolved CO_2 at equilibrium with the atmosphere at a given temperature. The transfer velocity k_{CO2} defines the speed at which CO_2 evades, and it is a function of water discharge (21), and thus it is affected by the hydropeaking regime. The supersaturation of dissolved CO_2 controls the maximum evasion (46).

From the CO_2 concentration and the hydraulic property of the river we calculated the CO_2 flux from the Zambezi River at Siavonga, 3 km downstream of Kariba Dam. We calculated the gas-transfer velocity using the empirical models from Raymond et al. (21), valid for large rivers characterized by low energy dissipation rates and in the absence of rapids (47, 48). We chose three models that require as input only the velocity and the slope of the river (models 3, 4, and 6; we discarded model 5 because the resulting velocity of exchange was much higher than the other models and thus a less conservative choice). The resulting k_{600} ranges between 0.7 and 1.4 $m \cdot d^{-1}$, and k_{CO2} is reported in *SI Appendix*, Fig. S4. We calculated the water flow velocity by running the one-dimensional steady version of Hec-Ras model for the Zambezi River downstream of Kariba Dam at different water discharges for the Zambezi River stretch from Kariba Dam to Chirundu (75 km downstream of Kariba Dam). We used cross-sections from Matos 2014 (49) estimated taking into account satellite images combined with the information of the simultaneous discharge in the river. The resulting longitudinal river slope is about 1.8×10^{-4}. Using this model, we derived the discharge velocity, the discharge-water depth, and the discharge-water surface width relationships at Siavonga (3 km downstream of Kariba Dam) needed for the calculation of CO_2 flux.

Data Availability. Time series and samples data have been deposited in the ETH Research Collection (DOI: 10.3929/ethz-b-000473097) (40).

ACKNOWLEDGMENTS. This project has received funding by the European Union's Horizon 2020 research and innovation program under grant agreement 690268 of the DAFNE project. We are grateful to Imasiku Nyambe (University of Zambia) for supporting communication with local partners, the Zambezi River Authority, ZESCO, and ZPC for sharing their data and useful information about the hydropower production. We also acknowledge Maurice Diamond for hosting and helping us conduct the field campaign around Kariba Dam, Christian Dinkel and Davide Vanzo for their support in the field, and Giulia Calamita for helping with the visualizations. A.S. acknowledges financial support from the Italian Ministry of Education, University and Research via the Departments of Excellence initiative 2018–2022 attributed to the Department of Civil, Environmental and Mechanical Engineering of the University of Trento (grant L. 232/2016).

1. T. J. Battin *et al.*, The boundless carbon cycle. *Nat. Geosci.* **2**, 598–600 (2009).
2. J. J. Cole *et al.*, Plumbing the global carbon cycle: Integrating inland waters into the terrestrial carbon budget. *Ecosystems* **10**, 172–185 (2007).
3. P. A. Raymond *et al.*, Global carbon dioxide emissions from inland waters. *Nature* **503**, 355–359 (2013).
4. R. Lauerwald, J. Hartmann, N. Moosdorf, S. Kempe, P. A. Raymond, What controls the spatial patterns of the riverine carbonate system? — A case study for North America. *Chem. Geol.* **337-338**, 114–127 (2013).
5. R. Lauerwald, G. G. Laruelle, J. Hartmann, P. Ciais, P. A. G. Regnier, Spatial patterns in CO_2 evasion from the global river network. *Global Biogeochem. Cycles* **29**, 534–554 (2015).
6. A. Rinaldo, M. Gatto, I. Rodriguez-Iturbe, *River Networks as Ecological Corridors: Species, Populations, Pathogens* (Cambridge University Press, 2020).
7. P. Regnier *et al.*, Anthropogenic perturbation of the carbon fluxes from land to ocean. *Nat. Geosci.* **6**, 597–607 (2013).
8. B. R. Deemer *et al.*, Greenhouse gas emissions from reservoir water surfaces: A new global synthesis. *Bioscience* **66**, 949–964 (2016).
9. Y. T. Prairie *et al.*, Greenhouse gas emissions from freshwater reservoirs: What does the atmosphere see? *Ecosystems* **21**, 1058–1071 (2018).
10. C. Zarfl, A. E. Lumsdon, J. Berlekamp, L. Tydecks, K. Tockner, A global boom in hydropower dam construction. *Aquat. Sci.* **77**, 161–170 (2015).
11. E. F. Moran, M. Claudia Lopez, N. Moore, N. Müller, D. W. Hyndman, Sustainable hydropower in the 21st century. *Proc. Natl. Acad. Sci. U.S.A.* **115**, 11891–11898 (2018).
12. G. Abril *et al.*, Carbon dioxide and methane emissions and the carbon budget of a 10-year old tropical reservoir (Petit Saut, French Guiana). *Global Biogeochem. Cycles* **19**, GB4007 (2005).
13. F. Guérin *et al.*, Methane and carbon dioxide emissions from tropical reservoirs: Significance of downstream rivers. *Geophys. Res. Lett.* **33**, L21407 (2006).
14. A. Kemenes, B. R. Forsberg, J. M. Melack, Downstream emissions of CH_4 and CO_2 from hydroelectric reservoirs (Tucuruí, Samuel, and Curuá-Una) in the Amazon Basin. *Inland Waters* **6**, 295–302 (2016).
15. C. Soued, Y. T. Prairie, The carbon footprint of a Malaysian tropical reservoir: Measured versus modelled estimates highlight the underestimated key role of downstream processes. *Biogeosciences* **17**, 515–527 (2020).
16. A. Maeck *et al.*, Sediment trapping by dams creates methane emission hot spots. *Environ. Sci. Technol.* **47**, 8130–8137 (2013).
17. M. S. Bevelhimer, A. J. Stewart, A. M. Fortner, J. R. Phillips, J. J. Mosher, CO_2 is dominant greenhouse gas emitted from six hydropower reservoirs in southeastern United States during peak summer emissions. *Water* **8**, 15 (2016).
18. C. Duvert, D. E. Butman, A. Marx, O. Ribolzi, L. B. Hutley, CO_2 evasion along streams driven by groundwater inputs and geomorphic controls. *Nat. Geosci.* **11**, 813–818 (2018).
19. R. S. Winton, E. Calamita, B. Wehrli, Reviews and syntheses: Dams, water quality and tropical reservoir stratification. *Biogeosciences* **16**, 1657–1671 (2019).
20. M. Carolli *et al.*, A simple procedure for the assessment of hydropeaking flow alterations applied to several European streams. *Aquat. Sci.* **77**, 639–653 (2015).
21. P. A. Raymond *et al.*, Scaling the gas transfer velocity and hydraulic geometry in streams and small rivers. *Limnol. Oceanogr. Fluid. Environ.* **2**, 41–53 (2012).
22. C. R. Teodoru *et al.*, Dynamics of greenhouse gases (CO_2, CH_4, N_2O) along the Zambezi River and major tributaries, and their importance in the riverine carbon budget. *Biogeosciences* **12**, 2431–2453 (2015).
23. T. DelSontro, K. K. Perez, S. Sollberger, B. Wehrli, Methane dynamics downstream of a temperate run-of-the-river reservoir. *Limnol. Oceanogr.* **61**, S188–S203 (2016).

Downloaded by guest on June 14, 2021

24. M. J. Kunz *et al.*, Sediment accumulation and carbon, nitrogen, and phosphorus deposition in the large tropical reservoir Lake Kariba (Zambia/Zimbabwe). *J. Geophys. Res.* **116**, G03003 (2011).
25. A. Zuijdgeest, B. Wehrli, Carbon and nutrient fluxes from floodplains and reservoirs in the Zambezi basin. *Chem. Geol.* **467**, 1–11 (2017).
26. E. Calamita *et al.*, Sixty years since the creation of Lake Kariba: Thermal and oxygen dynamics in the riverine and lacustrine sub-basins. *PloS One* **14**, e0224679 (2019).
27. A. Zuijdgeest, S. Baumgartner, B. Wehrli, Hysteresis effects in organic matter turnover in a tropical floodplain during a flood cycle. *Biogeochemistry* **131**, 49–63 (2016).
28. G. Zolezzi, A. Siviglia, M. Toffolon, B. Maiolini, Thermopeaking in alpine streams: Event characterization and time scales. *Ecohydrology* **4**, 564–576 (2011).
29. D. Vanzo, A. Siviglia, M. Carolli, G. Zolezzi, Characterization of sub-daily thermal regime in alpine rivers: Quantification of alterations induced by hydropeaking. *Hydrol. Process.* **30**, 1052–1070 (2015).
30. B. Wehrli, Conduits of the carbon cycle. *Nature* **503**, 346–347 (2013).
31. T. DelSontro *et al.*, Spatial heterogeneity of methane ebullition in a large tropical reservoir. *Environ. Sci. Technol.* **45**, 9866–9873 (2011).
32. R. M. Almeida *et al.*, Hydropeaking operations of two run-of-river mega-dams alter downstream hydrology of the largest amazon tributary. *Front. Environ. Sci.* **8**, 120 (2020).
33. L. Nyanti *et al.*, Physicochemical parameters and fish assemblages in the downstream river of a tropical hydroelectric dam subjected to diurnal changes in flow. *Int. J. Ecol.* **2018**, 1–9 (2018).
34. F. Colas *et al.*, Spatial and temporal variability of diffusive CO_2 and CH_4 fluxes from the Amazonian reservoir Petit-Saut (French Guiana) reveals the importance of allochthonous inputs for long-term C emissions. *Global Biogeochem. Cycles* **34**, e2020GB006602 (2020).
35. G. Myhre *et al.*, *Anthropogenic and Natural Radiative Forcing* (Cambridge University Press, Cambridge, UK, 2013), pp. 659–740.
36. A. Maeck, H. Hofmann, A. Lorke, Pumping methane out of aquatic sediments–Ebullition forcing mechanisms in an impounded river. *Biogeosciences* **11**, 2925–2938 (2014).
37. J. A. Harrison, B. R. Deemer, M. K. Birchfield, M. T. O'Malley. Reservoir water-level drawdowns accelerate and amplify methane emission. *Environ. Sci. Technol.* **51**, 1267–1277 (2017).
38. A. K. Sieczko *et al.*, Diel variability of methane emissions from lakes. *Proc. Natl. Acad. Sci. U.S.A.* **117**, 21488–21494 (2020).
39. E. Calamita, D. Vanzo, B. Wehrli, M. Schmid, Lake modelling reveals management opportunities for improving water quality downstream of transboundary tropical dams. *Water Resour. Res.* **57**, e2020WR027465 (2021).
40. E. Calamita, R. S. Winton, C. R. Teodoru, B. Wehrli, Water quality field campaign in the Zambezi River Basin. ETH Research Collection. https://www.research-collection.ethz.ch/handle/20.500.11850/473097. Deposited 4 March 2021.
41. R.F. Weiss, Carbon dioxide in water and seawater: The solubility of a non-ideal gas. *Mar. Chem.* **2**, 203–215 (1974).
42. A. D. Kney, D. Brandes, A graphical screening method for assessing stream water quality using specific conductivity and alkalinity data. *J. Environ. Manag.* **82**, 519–528 (2007).
43. M. Y. Thompson, D. Brandes, A. D. Kney, Using electronic conductivity and hardness data for rapid assessment of stream water quality. *J. Environ. Manag.* **104**, 152–157 (2012).
44. S. Van Heuven, D. Pierrot, J. W. B. Rae, E. Lewis, D. W. R. Wallace. CO2SYS v 1.1: MATLAB program developed for CO_2 system calculations (*ORNL/CDIAC-105b*, Carbon Dioxide Information Analysis Center, Oak Ridge National Laboratory, Oak Ridge, TN, 2011).
45. G. Abril *et al.*, Technical note: Large overestimation of pCO_2 calculated from pH and alkalinity in acidic, organic-rich freshwaters. *Biogeosciences* **12**, 67–78 (2015).
46. G. Rocher-Ros, R. A. Sponseller, W. Lidberg, C.-M. Mörth, R. Giesler, Landscape process domains drive patterns of CO_2 evasion from river networks. *Limnol. Oceanogr. Lett.* **4**, 87–95 (2019).
47. A. J. Ulseth *et al.*, Distinct air-water gas exchange regimes in low-and high-energy streams. *Nat. Geosci.* **12**, 259–263 (2019).
48. R. O. Hall, Jr, T. A. Kennedy, J. EmmaRosi-Marshall, Air-water oxygen exchange in a large whitewater river. *Limnol. Oceanogr. Fluid. Environ.* **2**, 1–11 (2012).
49. J. P. Matos, "Hydraulic-hydrologic model for the Zambezi River using satellite data and artificial intelligence techniques" (Technical report, EPFL, 2014).

Downloaded by guest on June 14, 2021